SIAM J. IMAGING SCIENCES
Vol. 7, No. 1, pp. 366–390

Image Restoration Using One-Dimensional Sobolev Norm Profiles of Noise and Texture*

Yunho Kim†, John B. Garnett‡, and Luminita A. Vese‡

Abstract. This work is devoted to image restoration (denoising and deblurring) by variational models. As in our prior work [*Inverse Probl. Imaging*, 3 (2009), pp. 43–68], the image $\tilde{f}$ to be restored is assumed to be the sum of a cartoon component u (a function of bounded variation) and a texture component v (an oscillatory function in a Sobolev space with negative degree of differentiability). In order to separate noise from texture in a blurred noisy textured image, we need to collect some information that helps distinguish noise, especially Gaussian noise, from texture. We know that homogeneous Sobolev spaces of negative differentiability help capture oscillations in images very well; however, these spaces do not directly provide clear distinction between texture and noise, which is also highly oscillatory, especially when the blurring effect is noticeable. Here, we propose a new method for distinguishing noise from texture by considering a family of Sobolev norms corresponding to noise and texture. It turns out that the two Sobolev norm profiles for texture and noise are different, and this enables us to better separate noise from texture during the deblurring process.

Key words. image restoration, image decomposition, convex optimization, Sobolev spaces

AMS subject classifications. 49N45, 49J40, 46N10, 65K10

DOI. 10.1137/130911275

1. Introduction.

We consider in this paper one of the classical problems in image analysis: the recovery of an unknown image from its blurry-noisy version, in the presence of a known blurring operator K. Assume we are given a blurry-noisy grayscale image $f : \mathbb{R}^n \to \mathbb{R}$ (if the image is only defined on a bounded domain Ω, such as a rectangle in $\mathbb{R}^2$, we extend it by zero or by periodicity on the complement $\mathbb{R}^n \setminus \Omega$):

$$f = K\tilde{f} + \text{noise}.$$

In our proposed method, we not only recover the sharp image $\tilde{f}$, but also decompose $\tilde{f}$ into its cartoon and texture parts, which will be denoted by u and v, respectively.

The standard method for solving such inverse ill-posed problems is inspired by Tikhonov regularization [49], [50], [51], which can be regarded as a general minimization problem of a

*Received by the editors February 26, 2013; accepted for publication (in revised form) October 21, 2013; published electronically February 20, 2014. This work was supported by National Science Foundation grants NSF DMS-0714945 and DMS-1217239, by the Institute for Pure and Applied Mathematics, and by a Beckenbach Dissertation Year Fellowship. A very preliminary and short version of this work was presented at the 18th IEEE International Conference on Image Processing (see [25]).
http://www.siam.org/journals/siims/7-1/91127.html

†Department of Diagnostic Radiology, Yale University, New Haven, CT 06520 (yunho.kim@yale.edu).
‡Department of Mathematics, University of California, Los Angeles, CA 90095 (jbg@math.ucla.edu, lvese@math.ucla.edu).

functional in integral form,

$$\inf_{\tilde{f}} \int |f - K\tilde{f}|^p dx + \lambda \int R(\tilde{f}) dx, \tag{1.1}$$

where p depends on the type of noise (for instance, $p = 2$ for Gaussian noise, while $p = 1$ for Laplacian or impulse noise). The regularizing potential R usually has the form $R(\tilde{f}) = R(|D\tilde{f}|)$, so that it depends on the partial derivatives of $\tilde{f}$. We assume that R has at most linear growth at infinity to facilitate the recovery of sharp edges. Earlier work on variational image deblurring includes a study of the Wiener filter with quadratic potential [22], the work of Geman and Geman [20] with nonconvex potentials in the discrete setting, and the work of Rudin and Osher [43] (as an extension of [44] to deblurring) in the continuous and discrete cases when the regularization is the total variation. We also refer to extensive works on minimization models of the form (1.1), with theoretical results, numerical algorithms, and experimental results: [1], [13], [7], [52], [4] for the analysis of the problem in the convex case; [17], [11], [10] with convex or nonconvex regularizations; and [33], [35], [36], [16] using total variation and wavelet principles.

In the last several years, model (1.1) has been generalized to cases of the form

$$\inf_{\tilde{f}} \|f - K\tilde{f}\|^p + \lambda \int R(|D\tilde{f}|), \tag{1.2}$$

where $\|\cdot\|$ denotes the norm in a Banach space of generalized functions of negative degree of differentiability, which better model oscillatory functions (such as noise or texture). This is inspired by work of Meyer [37] and of Mumford and Gidas [38]. When $K = I$, spaces of negative differentiability were used both theoretically and numerically to model oscillatory functions and to separate cartoon from texture; for examples, see [53], [41]; work by Aujol and coworkers [8], [9], [6]; Le and Vese [29]; Garnett and coworkers [19], [18]; Starck, Elad, and Donoho [45]; Levine [30]; or a hierarchical approach in Tadmor, Nezzar, and Vese [46].

A Sobolev space of distributions of negative differentiability for image deblurring has been used in [41], where it is imposed that $\tilde{f} \in BV$ and $f - K\tilde{f} \in \dot{H}^{-1}$. This was generalized in [32] to the case $\tilde{f} \in BV$ and $f - K\tilde{f} \in \dot{H}^{-s}$ $(s > 0)$, a Sobolev space defined via the Fourier transform. In these works, the recovered image $\tilde{f}$ is represented by a function of bounded variation. However, the use of BV ignores many oscillatory details, such as texture. Indeed, it has been shown in [23], [2], and [3] that natural images with fine details are not well represented by functions of bounded variation.

To better restore images including texture and details (that are not necessarily modeled by functions of bounded variation), several recent papers have appeared that propose several different methods. We mention some of them below:

(ia) Hierarchical decompositions were used to better recover images with small details and texture for deblurring in the presence of noise. See, for example, Tadmor, Nezzar, and Vese [46], [47] and Athavale and Tadmor [5].

(ib) Variational proximal point methods for solving ill-posed inverse problems such as deblurring in the presence of noise (work by Osher et al. [40], etc.)

(ii) Methods using patch-based techniques and nonlocal operators (such as NL Means by Buades, Coll, and Morel [12] and Kindermann, Osher, and Jones [28], or nonlocal total

variation [21] by Gilboa and Osher) were extended to image deblurring for better restoration of texture. We would like to mention the work of Lou et al. [34], Peyré, Bougleux, and Cohen [42], and Jung and Vese [24], among others.

(iii) Deblurring using regularized locally adaptive kernel regression–based methods in the presence of noise, by Takeda, Farsiu, and Milanfar [48].

(iv) Finally, work aiming to recover the unknown image $\tilde{f}$ using the cartoon + texture model $u+v$. Here the first work is by Daubechies and Teschke [14], where the authors recover an image from its blurry version by the following "cartoon + texture" minimization model:

$$\inf_{u\in B^1_{1,1}, v\in H^{-1}} \mu\|f - K(u+v)\|_{L^2}^2 + |u|_{B^1_{1,1}} + \lambda\|v\|_{H^{-1}}^2 \tag{1.3}$$

in the Besov-wavelets framework. Very satisfactory results are reported in [14], where the recovered sharp image is given by $\tilde{f} = u + v$. A second model for image restoration using cartoon and texture, which forms a basis for the one presented here, is introduced and analyzed in [27] (as an extension of model [18] to deblurring):

$$\inf_{u\in BV, v\in \dot{W}^{-s,p}} \mu\|f - K(u+v)\|_{L^2}^2 + |u|_{BV} + \lambda\|v\|_{\dot{W}^{-s,p}}.$$

Our proposed work is a continuation of [27]. In the present paper, using one-dimensional profiles of Sobolev norms of negative degree of differentiability, we distinguish noise from texture in the restoration model. (Otherwise, both noise and texture could be captured in the same component, especially when the noise is strong.) We first describe the main idea and the proposed variational model. We analyze theoretically the variational model, showing existence of minimizers. Then we give the derivation details of the Euler–Lagrange equations and of the numerical algorithm. Finally, we present numerical results for image deblurring in the presence of noise obtained by the proposed model. Comparisons with state-of-the-art results found in [24] show that the proposed model gives improved results.

2. Proposed model.

2.1. One-dimensional Sobolev norm profiles of noise and texture. We assume that the noise n has a known PDF (probability density function); that is, at each point x, $n(x)$ is a random variable following a given PDF. For example, the PDF could be a Gaussian function with zero mean and known variance σ^2. For each function v, we define a function $\phi_v(\cdot)$ of $s \in \mathbb{R}_- = \{s \in \mathbb{R} : s < 0\}$ by

$$\phi_v(s) = \|(0.1 \cdot 2\pi|\xi|)^s \hat{v}(\cdot)\|_{L^2(\mathbb{R}^n)}, \tag{2.1}$$

where $\hat{v}$ is the Fourier transform of v.

Let us explain our choice of the constant $C = 0.1 \cdot 2\pi$ in the norm (2.1). For any constant $C > 0$, $\|(C|\xi|)^s \hat{v}(\cdot)\|_{L^2(\mathbb{R}^n)}$ defines a norm equivalent to the homogeneous Sobolev norm $\|v\|_{\dot{H}^s}$. But since we want to emphasize high frequencies, which serve to distinguish texture from noise, and since we will work with $s < 0$ and $|s|$ large, we may take $0 < C < 1$ in place of $0.1 \cdot 2\pi$, to give high frequencies more weight. The particular choice $0.1 \cdot 2\pi$ is for computational convenience and is fixed throughout the paper.

Let (a, b) be an interval in $\mathbb{R}_-$. The main assumption is that texture and noise have quite distinguishable homogeneous Sobolev norm profiles when a family of negative homogeneous Sobolev norms shown in (2.1) for $s \in (a, b)$ are considered simultaneously. Moreover, we assume that the function ϕ_v of $s \in \mathbb{R}_-$ behaves in the same way for all texture images v. We denote by T such a "universal" function describing this common behavior of ϕ_v. Likewise, we make the same assumption on ϕ_n; that is, when applied to noise n, the function ϕ_n depends only on the noise distribution. So, if two noise images n_1 and n_2 are from the same noise distribution, then $\phi_{n_1}(s) \approx \phi_{n_2}(s)$ for $s \in \mathbb{R}_-$. We denote by N such a universal function describing this common behavior of ϕ_n for Gaussian noise n in this work. We assume throughout this paper that T and N are known. This assumption was inspired by the experiments in Figure 1, where the computed one-dimensional profiles of $\phi_v(s)$ and $\phi_n(s)$ for $s < 0$ are given for several purely texture images v and one Gaussian noise image n. The x-axis represents s in an interval of negative values, while the y-axis represents the values of $\phi_v(s)$ and $\phi_n(s)$ for a given texture image v and the noise n. The texture profiles of ϕ_v are in red, and the noise profiles of ϕ_n are in blue. We note that for all six textured images shown, the red profiles for texture images are much different from the blue profiles for Gaussian noise, whereas the red profiles are similar in shape to one another. Even though the texture profiles, the red dashed lines in Figure 1, are similar in shape, their actual values are slightly different. Therefore we would like to develop a model that allows ϕ_v and ϕ_n to be somewhat different from T and N, but to be controlled by T and N in some way. In section 3, we describe how one can compute the two functions T and N to be used in the numerical experiments. We also show in Figure 2 two noisy images (constant images corrupted by additive Gaussian noise of different variances) and their Sobolev norm profiles.

In the image processing literature, dual Banach spaces have been frequently used to model oscillatory components. For instance, Meyer [37] considered the dual spaces $G \subset F \subset E$ of negative differentiability, where G is dual to the homogeneous Sobolev space $\dot{W}^{1,1}(\mathbb{R}^2)$, F can be expressed as $\operatorname{div}(B\dot{M}O(\mathbb{R}^2;\mathbb{R}^2))$, and, finally, $E = \dot{B}_\infty^{-1,\infty}(\mathbb{R}^2)$ is dual to the homogeneous Besov space $\dot{B}_1^{1,1}(\mathbb{R}^2)$. Among possible choices of dual spaces, we note that the Sobolev spaces $W^{s,p}, \dot{W}^{s,p}$ and the Besov spaces $B_q^{s,p}, \dot{B}_q^{s,p}$ depend on a parameter s that measures the degree of a distribution's differentiability. Hence, unlike previous attempts at modeling the oscillatory components of images in which a single dual space was used to model either texture or noise, we will use an entire family of dual spaces having a scaling parameter related to the degree of differentiability. In this paper, we will work only with Sobolev spaces, although Besov spaces could provide an alternative approach.

In the absence of blurring, it is less difficult to denoise noisy images. There are many efficient algorithms to remove noise, whether it is additive or multiplicative or of a more complex nature. However, many such algorithms are not well suited for a denoising + deblurring problem because the two processes, denoising and deblurring, are completely opposite in nature. In other words, denoising can be considered as a smoothing process, while deblurring can be considered as a sharpening process. Hence, when combined they compete with each other and produce a highly ill-posed problem. In most models stronger deblurring may also amplify the noise and instabilities. Here we will use the additional information presented above to better recover natural textured images corrupted by both blur and noise.

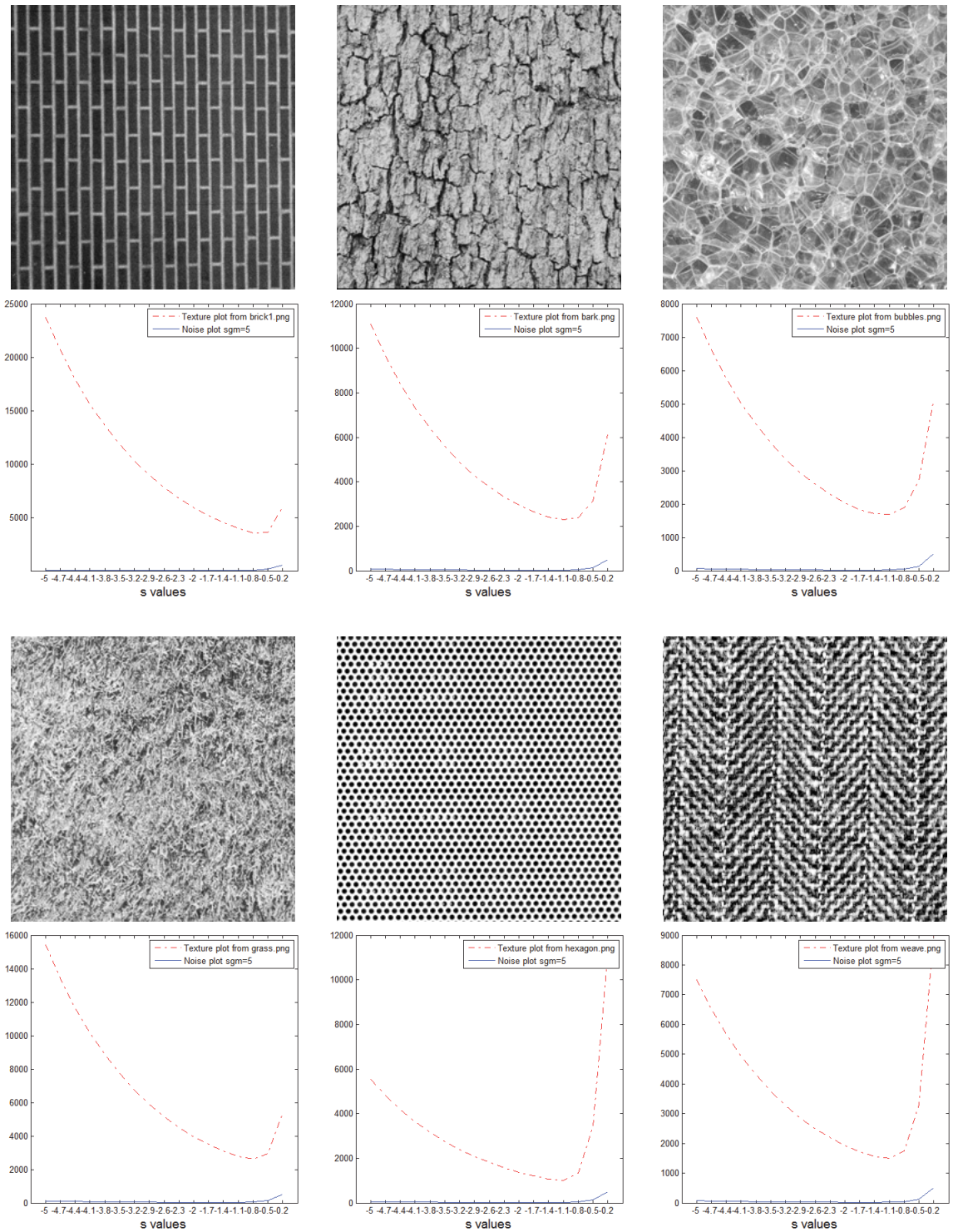

Figure 1. *Texture images v and their Sobolev norm profiles ϕ_v, together with noise profile ϕ_n. In each plot, the red dotted line is the Sobolev profile of the texture image above; the blue solid line is the noise Sobolev profile. The s values are between -5.4 and -0.2.*

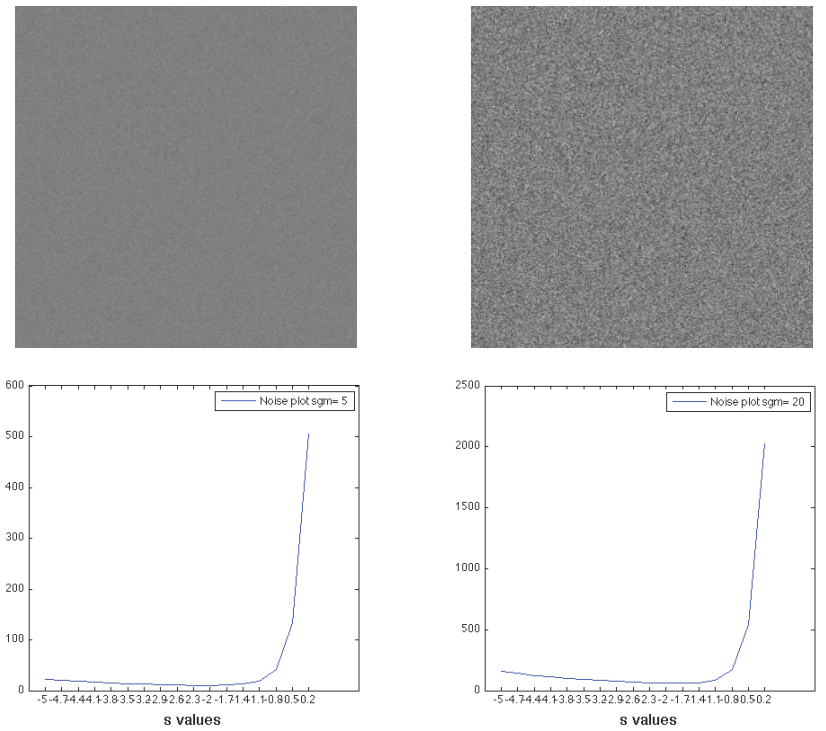

Figure 2. *Two Gaussian noise images of different variances and their Sobolev norm profiles.*

2.2. Description of the proposed image restoration model. As a continuation of the work [27], we may consider the following minimization problem to incorporate a series of Sobolev spaces:

$$\min_{u,v}\Big\{|u|_{\mathcal{BV}}+\lambda\|f-k*(u+v)\|_{L^2}^2 + \frac{\mu}{b-a}\|T-\phi_v\|_{L^2(a,b)}^2+\frac{\gamma}{b-a}\|N-\phi_{f-k*(u+v)}\|_{L^2(a,b)}^2\Big\}, \tag{2.2}$$

with $a<b<0$.

The function ϕ_v was defined in (2.1), and we use $k*(u+v)$ here and in what follows to realize the blurring operator K by a convolution operator with a kernel k, i.e., $K(u+v)=k*(u+v)$. In the above minimization model, f is a given blurry and noisy datum; the recovered image will be represented by $u+v$; if (u,v) would be a minimizing pair of the above functional, then the recovered texture component v must have its Sobolev profile similar to the universal texture profile $T(s)$, while the computed noise residual $f-k*(u+v)$ must have its Sobolev profile close to the universal Gaussian noise profile $N(s)$. In practice, the universal learned texture profile T is an average of profiles corresponding to several different purely texture images, and N will be obtained in the same way with several purely noise images with a prescribed variance; λ, μ, and γ are positive coefficients. We also impose that the cartoon component u is of bounded variation.

As described earlier, we want to consider a series of homogeneous Sobolev spaces $\dot{W}^{s,p}$ for $s < 0$. We no longer restrict ourselves to the case $-2 \leq s < 0$ as in [18], [19].

Unfortunately, the functional in (2.2) is not convex. Moreover, in this model, we assume the existence of the two functions $T(s)$ and $N(s)$ while imposing that minimizers (u, v) should have $\phi_v(s)$ and $\phi_{f-k*(u+v)}$ close to $T(s)$ and $N(s)$, respectively. But in practice such universal functions T and N are not fully known; we only estimate them by considering a few texture and noise images. Thus we know only probable profiles of T and N, and not their exact profiles. Hence, knowing that recovering details of v requires v to contain more structured oscillatory components, we would like to use T and N not necessarily for perfect matches of ϕ_v and ϕ_n, but for upper bounds of ϕ_v and ϕ_n, respectively, so that we can recover as much detail as possible up to T and as much noise as possible up to N. In this spirit, we also propose the following convex constrained minimization problem that can be seen as a relaxed version of the previous nonconvex model.

Proposed constrained minimization problem: We define $\mathcal{F}$ by

$$\mathcal{F}(u, v) = |u|_{\mathcal{BV}} + \lambda \|f - k * (u + v)\|_{L^2}^2$$

and propose to solve

$$\inf_{u,v} \mathcal{F}(u, v), \tag{2.3}$$

subject to

$$\phi_v \leq T \quad \text{and} \quad \phi_{f-k*(u+v)} \leq N \qquad \text{a.e. in } (a, b),$$

in appropriate spaces for u and v that will be described later.

Remark 1. $\mathcal{F}$ is convex in u and v, and the feasible set

$$E = \{(u, v) : \phi_v \leq T \text{ and } \phi_{f-k*(u+v)} \leq N \text{ a.e. in } (a, b)\}$$

is also convex.

We now proceed with a series of definitions of function spaces that we will use. Since the case $n = 1$ is more trivial than the other cases $n \geq 2$, we will make the assumption $n \geq 2$, and our main interest is the case $n = 2$.

Definition 2.1 (BV space). *$BV(\mathbb{R}^n)$ for $n \geq 2$ is the space of functions of bounded variation; i.e., $u \in BV(\mathbb{R}^n)$, if and only if $u \in L^1(\mathbb{R}^n)$ and there exists a Radon measure Du that is a gradient of u in the distributional sense with total variation*

$$\int_{\mathbb{R}^n} |Du| := \sup \left\{ \int_{\mathbb{R}^n} u \operatorname{div}(\phi) dx : \ \phi \in C_c^1(\mathbb{R}^n, \mathbb{R}^n), \ \|\phi\|_\infty \leq 1 \right\} < \infty.$$

Remark 2. The space $W^{1,1}(\mathbb{R}^n)$ is a subspace of $BV(\mathbb{R}^n)$, and for $u \in W^{1,1}(\mathbb{R}^n)$ we have $\int_{\mathbb{R}^n} |Du| = \int_{\mathbb{R}^n} |\nabla u(x)| dx$, where Du is the usual gradient ∇u in $L^1(\mathbb{R}^n, \mathbb{R}^n)$. The Banach space $BV(\mathbb{R}^n)$ is equipped with the following norm, which extends the classical norm in $W^{1,1}(\mathbb{R}^n)$:

$$\|u\|_{BV(\mathbb{R}^n)} = \|u\|_{L^1(\mathbb{R}^n)} + \int_{\mathbb{R}^n} |Du|.$$

In this paper, we will use a slightly different space to model the cartoon component. The following definition can be found in [37]. To distinguish it from the classical BV space, $BV(\mathbb{R}^n)$, we denote it by $\mathcal{BV}(\mathbb{R}^n)$.

Definition 2.2. *$\mathcal{BV}(\mathbb{R}^n)$ for $n \geq 2$ is the space of functions u satisfying the following:*

1. *u vanishes at infinity in a weak sense; that is, $u * \varphi(x) \to 0$ as $|x| \to \infty$ for $\varphi \in \mathcal{S}(\mathbb{R}^n)$.*
2. *The distributional gradient Du of the function u is a bounded Radon measure.*

Remark 3. $\mathcal{S}(\mathbb{R}^n)$ is the Schwartz space. Note that any function in $L^p(\mathbb{R}^n)$, $1 \leq p < \infty$, vanishes at infinity in the weak sense described above.

Theorem 2.3. *$\mathcal{BV}(\mathbb{R}^n)$ is a Banach space with a norm $|u|_{\mathcal{BV}}$ defined by*

$$\|u\|_{\mathcal{BV}} = \|Du\|(\mathbb{R}^n) = \int_{\mathbb{R}^n} |Du|.$$

In fact, $\mathcal{BV}(\mathbb{R}^n)$ is the dual space of Γ with the dual norm, where Γ is a Banach space defined by

$$\Gamma = \{f \in \mathcal{S}'(\mathbb{R}^n) : f = \partial_1 g_1 + \cdots + \partial_n g_n,\ g_i \in C_0(\mathbb{R}^n)\}$$

with the norm

$$\|f\|_\Gamma = \inf\{\sqrt{|g_1|^2 + \cdots + |g_n|^2} : f = \partial_1 g_1 + \cdots + \partial_n g_n\}.$$

Proof. We refer to [37] for the proof. ∎

Note that the norm $\|\cdot\|_{\mathcal{BV}}$ is the same as the usual seminorm $|\cdot|_{BV}$, and this Banach space $\mathcal{BV}(\mathbb{R}^n)$ is more useful than $BV(\mathbb{R}^n)$ in that it encompasses more functions, yet it has the continuous embedding

$$\|u\|_{L^{n/(n-1)}} \lesssim \|u\|_{\mathcal{BV}}$$

for $n \geq 2$.

Definition 2.4. *For $s \in \mathbb{R}$, we define the Sobolev space $H^s(\mathbb{R}^n)$ by*

$$H^s(\mathbb{R}^n) = \left\{ \overline{f \in \mathcal{S}(\mathbb{R}^n) : \int_{\mathbb{R}^n} (1 + |\xi|^2)^s |\hat{f}(\xi)|^2 d\xi < \infty} \right\}$$

with the norm

$$\|f\|_{H^s} = \left(\int_{\mathbb{R}^n} (1 + |\xi|^2)^s |\hat{f}(\xi)|^2 d\xi \right)^{1/2},$$

and its homogeneous version $\dot{H}^s(\mathbb{R}^n)$ by

$$\dot{H}^s(\mathbb{R}^n) = \left\{ \overline{f \in \mathcal{S}_0(\mathbb{R}^n) : \int_{\mathbb{R}^n} |\xi|^{2s} |\hat{f}(\xi)|^2 d\xi < \infty} \right\},$$

where $\mathcal{S}_0(\mathbb{R}^n)$ is the set of Schwartz functions whose Fourier transforms vanish near the origin, with the norm

$$\|f\|_{\dot{H}^s} = \left(\int_{\mathbb{R}^n} |\xi|^{2s} |\hat{f}(\xi)|^2 d\xi \right)^{1/2}.$$

Remark 4. We use the homogeneous space $\dot{H}^s(\mathbb{R}^n)$ to avoid certain unnecessary and technical difficulties.

Theorem 2.5. *$H^s(\mathbb{R}^n), \dot{H}^s(\mathbb{R}^n)$ for $s \in \mathbb{R}$ are Hilbert spaces with inner products $\langle\ ,\ \rangle_{H^s}$ and $\langle\ ,\ \rangle_{\dot{H}^s}$, respectively, defined by*

$$\langle f, g \rangle_{H^s} = \int_{\mathbb{R}^n} (1 + |\xi|^2)^s \hat{f}(\xi) \bar{\hat{g}}(\xi) d\xi,$$
$$\langle f, g \rangle_{\dot{H}^s} = \int_{\mathbb{R}^n} |\xi|^{2s} \hat{f}(\xi) \bar{\hat{g}}(\xi) d\xi.$$

Proof. This proof is an easy exercise and can be found in many textbooks. ∎

In this paper, we will particularly use the following property.

Theorem 2.6. *$\dot{H}^s(\mathbb{R}^n)$ is the dual space of $\dot{H}^{-s}(\mathbb{R}^n)$ for $s < 0$.*

With the appropriate choices of spaces above, we can now prove the existence of a minimizer of the problem (2.3).

Theorem 2.7. *Let $a < b < 0$, $n \geq 2$, and $\lambda > 0$. We assume that the blurring kernel k belongs to $L^{\frac{2n}{n+2}}(\mathbb{R}^n)$ and that there exists $s_1 \in (a, b)$ such that the Fourier transform $\hat{k}$ satisfies $\| |\cdot|^{-s_1} \hat{k}(\cdot) \|_{L^\infty(\mathbb{R}^n)} < \infty$. We also assume that $T, N \in L^2(a, b)$ and $T > 0, N > 0$ a.e. in (a, b). If there exists $(u^*, v^*) \in \mathcal{BV}(\mathbb{R}^n) \times \cap_{a<s<b} \dot{H}^s(\mathbb{R}^n)$ satisfying the constraints with $\mathcal{F}(u^*, v^*) < \infty$ in (2.3)—in other words, if the feasible set is nonempty—then (2.3) has a minimizer in $\mathcal{BV}(\mathbb{R}^n) \times \cap_{a<s<b} \dot{H}^s(\mathbb{R}^n)$.*

Remark 5. The condition on the Fourier transform $\hat{k}$ that $\| |\cdot|^{-s_1} \hat{k}(\cdot) \|_{L^\infty(\mathbb{R}^n)} < \infty$ for some $s_1 \in (a, b)$ is not a restriction in many applications: any Gaussian or averaging kernel satisfies the condition with $a < -1 < b < 0$. Moreover, having a nonempty feasible set is not a restriction either because we are free to choose T and N in $L^2(a, b)$.

Proof. Throughout the proof, we may ignore the constant $C > 0$ introduced when defining the function $\phi_v(s)$, which is equivalent to the homogeneous Sobolev norm $\|v\|_{\dot{H}^s}$. The restriction $0 < C < 1$ is important only for the numerical experiments. Hence, we will simply use $\|\cdot\|_{\dot{H}^s}$ for $\phi_{\{\cdot\}}(s)$ during this proof. Thus, we will replace $\phi_v(s)$ and $\phi_{f-k*(u+v)}(s)$ by $\|v\|_{\dot{H}^s}$ and $\|f - k * (u + v)\|_{\dot{H}^s}$, respectively.

For simplicity, we write $\{\alpha_n\}$ for both a sequence and for one of its subsequences. Also we use the simpler notation $\mathcal{S}, \mathcal{S}', BV, \mathcal{BV}, \dot{H}^s, L^2$ for the spaces described above.

Let $\{(u_k, v_k)\}_{k=1}^\infty$ be a minimizing sequence of (2.3). Then there exists $0 < M < \infty$ such that for all $k \geq 1$,

$$\mathcal{F}(u_k, v_k) < M,$$

because, by assumption, $\mathcal{F}(u^*, v^*) < \infty$ for some (u^*, v^*) and we may set $M = \mathcal{F}(u^*, v^*)$.

Since for any $k \geq 1$, $\|v_k\|_{\dot{H}^s} = \phi_{v_k}(s) \leq T(s)$ for almost every $s \in (a, b)$, we know that

$$\left(\int_a^b \|v_k\|_{\dot{H}^s}^2 ds \right)^{1/2} = \|\phi_{v_k}\|_{L^2(a,b)} \leq \|T\|_{L^2(a,b)}.$$

Then for any $s \in (a,b)$, there exists $\epsilon > 0$ such that $(s-\epsilon, s+\epsilon) \subset (a,b)$, and we can obtain

$$\begin{aligned}\epsilon\|v_k\|_{\dot{H}^s}^2 &= (s-(s-\epsilon))\int_{|\xi|\le 1}|\hat{v_k}(\xi)|^2|\xi|^{2s}d\xi + ((s+\epsilon)-s)\int_{|\xi|>1}|\hat{v_k}(\xi)|^2|\xi|^{2s}d\xi \\ &\le \int_{s-\epsilon}^{s}\int_{|\xi|\le 1}|\hat{v_k}(\xi)|^2|\xi|^{2t}d\xi dt + \int_{s}^{s+\epsilon}\int_{|\xi|>1}|\hat{v_k}(\xi)|^2|\xi|^{2t}d\xi dt \\ &\le \int_{s-\epsilon}^{s+\epsilon}\|v_k\|_{\dot{H}^t}^2 dt \le \|T\|_{L^2(a,b)}^2.\end{aligned}$$

Hence, for any $s \in (a,b)$, we have

$$\sup_{k\ge 1}\|v_k\|_{\dot{H}^s}^2 < \infty. \tag{2.4}$$

We now fix $s_0 \in (a,b)$. There exists $v_0 \in \dot{H}^{s_0}$ such that for any $h \in \dot{H}^{-s_0}$, up to a subsequence,

$$\lim_{k\to\infty}\langle h, v_k\rangle_{\dot{H}^{-s_0}\times\dot{H}^{s_0}} = \langle h, v_0\rangle_{\dot{H}^{-s_0}\times\dot{H}^{s_0}}.$$

In particular, if $h \in \dot{H}^{-s_0}\cap\dot{H}^{-s}$ for $s \in (a,b)$, then $\dot{H}^{-s_0}\cap\dot{H}^{-s}$ is dense in $\dot{H}^{-s}$ and

$$\lim_{k\to\infty}\langle h, v_k\rangle_{\dot{H}^{-s}\times\dot{H}^{s}} = \langle h, v_0\rangle_{\dot{H}^{-s}\times\dot{H}^{s}},$$

which means that, for $s \in (a,b)$, $v_0 \in \dot{H}^s$ and

$$\|v_0\|_{\dot{H}^s} \le \liminf_{k\to\infty}\|v_k\|_{\dot{H}^s}. \tag{2.5}$$

Hence, by Fatou's lemma, we obtain

$$\int_a^b \|v_0\|_{\dot{H}^s}^2 ds \le \liminf_{k\to\infty}\int_a^b \|v_k\|_{\dot{H}^s}^2 ds \le \|T\|_{L^2(a,b)}^2.$$

We now claim that

$$k * v_k \rightharpoonup k * v_0 \quad \text{in } L^2. \tag{2.6}$$

Let $h \in L^2$. Note that for $v \in \dot{H}^{s_1}$

$$|\langle k*v, h\rangle_{L^2}| \le \int_{\mathbb{R}^n}|\xi|^{s_1}|\hat{v}(\xi)||\xi|^{-s_1}|\hat{k}(\xi)||\hat{h}(\xi)|d\xi \le \||\xi|^{-s_1}\hat{k}(\xi)\|_{L^\infty}\|v\|_{\dot{H}^{s_1}}\|h\|_{L^2}.$$

This implies that

$$\lim_{k\to\infty}\langle k*v_k, h\rangle_{L^2} = \lim_{k\to\infty}\langle v_k, \tilde{k}*h\rangle_{\dot{H}^{s_1}\times\dot{H}^{-s_1}} = \langle v_0, \tilde{k}*h\rangle_{\dot{H}^{s_1}\times\dot{H}^{-s_1}} = \langle k*v_0, h\rangle_{L^2},$$

where $\tilde{k}(x) = k(-x)$ and $k * v_0 \in L^2$, which implies (2.6).

As for the sequence $\{u_k\}_{k=1}^{\infty}$, we already know that

$$\|u_k\|_{L^{\frac{n}{n-1}}} \lesssim \|u_k\|_{\mathcal{BV}} \leq M,$$

so that there exists $u_0 \in L^{\frac{n}{n-1}}$ such that, up to a subsequence,

$$u_k \rightharpoonup u_0 \quad \text{in } L^{\frac{n}{n-1}}. \tag{2.7}$$

We also claim that

$$k * u_k \rightharpoonup k * u_0 \quad \text{in } L^2. \tag{2.8}$$

To see this, we take $\varphi \in L^2$ and prove that a linear mapping $T_\varphi : L^{\frac{n}{n-1}} \to \mathbb{R}$ defined by

$$T_\varphi(u) = \int_{\mathbb{R}^n} \varphi(x) k * u(x) dx = \int_{\mathbb{R}^n} \tilde{k} * \varphi(x) u(x) dx$$

satisfies

$$|T_\varphi(u)| \lesssim \|\varphi\|_{L^2} \|u\|_{L^{\frac{n}{n-1}}}. \tag{2.9}$$

Then (2.9) together with (2.7) proves (2.8).

To prove (2.9) it is enough by the Plancherel theorem to show that

$$\int_{\mathbb{R}^n} |\hat{\varphi}(\xi)||\hat{k}(\xi)||\hat{u}(\xi)| d\xi \lesssim \|\varphi\|_{L^2} \|u\|_{L^{\frac{n}{n-1}}}. \tag{2.10}$$

Note that the Hausdorff–Young inequality says that for each $n \geq 2$

$$\|\hat{u}\|_{L^n} \lesssim \|u\|_{L^{\frac{n}{n-1}}} \quad \text{and} \quad \|\hat{k}\|_{L^{\frac{2n}{n-2}}} \lesssim \|k\|_{L^{\frac{2n}{n+2}}}.$$

If $n = 2$, then $2n/(n+2) = 1$ and $n/(n-1) = 2$. Hence, $\hat{k} \in L^\infty$ implies (2.10). If $n > 2$, then we obtain (2.10) by Hölder's inequality:

$$\begin{aligned}
\int_{\mathbb{R}^n} |\hat{\varphi}(\xi)||\hat{k}(\xi)||\hat{u}(\xi)| d\xi &\leq \left(\int_{\mathbb{R}^n} |\hat{\varphi}(\xi)|^{\frac{n}{n-1}} |\hat{k}(\xi)|^{\frac{n}{n-1}} d\xi \right)^{\frac{n-1}{n}} \|\hat{u}\|_{L^n} \\
&\lesssim \left(\int_{\mathbb{R}^n} |\hat{\varphi}(\xi)|^2 \right)^{\frac{1}{2}} \left(\int_{\mathbb{R}^n} |\hat{k}(\xi)|^{\frac{2n}{n-2}} \right)^{\frac{n-2}{2n}} \|u\|_{L^{\frac{n}{n-1}}} \\
&\lesssim \|\varphi\|_{L^2} \|u\|_{L^{\frac{n}{n-1}}}.
\end{aligned}$$

Hence, (2.8) holds, and if $\phi \in C_c^1$ with $\|\phi\|_\infty \leq 1$, then

$$\int_{\mathbb{R}^n} u_0 \cdot \operatorname{div} \phi = \lim_{k \to \infty} \int_{\mathbb{R}^n} u_k \cdot \operatorname{div} \phi \leq \liminf_{k \to \infty} \|u_k\|_{\mathcal{BV}}$$

implies

$$\|u_0\|_{\mathcal{BV}} \leq \liminf_{k \to \infty} \|u_k\|_{\mathcal{BV}}. \tag{2.11}$$

Therefore, $u_0 \in \mathcal{BV}$.

After extracting appropriate subsequences, we may now assume that the two sequences $\{u_k\}$, $\{v_k\}$ have weak limits u_0, v_0 satisfying (2.5)–(2.11).

It now follows easily from the arguments above that

$$\mathcal{F}(u_0, v_0) \le \mathcal{F}(u_k, v_k) \quad \text{for all } k \ge 1. \tag{2.12}$$

What remains to prove is that (u_0, v_0) satisfies the constraints. As a matter of fact, (2.5) implies that

$$\phi_{v_0} \le T \quad \text{a.e. in } (a, b).$$

We note that

$$f - k * u_k - k * v_k \rightharpoonup f - k * u_0 - k * v_0 \quad \text{in } L^2.$$

It can also be shown that for $s \in (a, b)$

$$\sup_{k \ge 1} \|f - k * u_k - k * v_k\|_{\dot{H}^s}^2 < \infty, \tag{2.13}$$

in the same way as (2.4) was shown. Let $h \in \mathcal{S}_0$. Then $h \in \dot{H}^t$ for $t > 0$. Hence, for $s \in (a, b)$

$$\begin{aligned}\lim_{k\to\infty} \langle f - k * u_k - k * v_k, h\rangle_{\dot{H}^s \times \dot{H}^{-s}} &= \lim_{k\to\infty} \langle f - k * u_k - k * v_k, h\rangle_{L^2} = \langle f - k * u_0 - k * v_0, h\rangle_{L^2} \\ &= \langle f - k * u_0 - k * v_0, h\rangle_{\dot{H}^s \times \dot{H}^{-s}}.\end{aligned}$$

Since such functions as h are densely distributed in $\dot{H}^{-s}$, we obtain that

$$f - k * u_k - k * v_k \rightharpoonup f - k * u_0 - k * v_0 \quad \text{in } \dot{H}^s,$$

which implies

$$\|f - k * (u_0 + v_0)\|_{\dot{H}^s} \le N \quad \text{a.e. in } (a, b).$$

Thus from (2.12) and the fact that $\{(u_k, v_k)\}_{k=1}^{\infty}$ is a minimizing sequence, we see that

$$(u_0, v_0) \in \mathcal{BV} \times \cap_{a<s<b} \dot{H}^s$$

is a minimizer. ■

Remark 6. The constraints in (2.3)

$$\phi_v \le T \quad \text{and} \quad \phi_{f-k*(u+v)} \le N \qquad \text{a.e. in } (a, b)$$

can be more relaxed to

$$\|\phi_v\|_{L^2(a,b)} \le \|T\|_{L^2(a,b)} \quad \text{and} \quad \|\phi_{f-k*(u+v)}\|_{L^2(a,b)} \le \|N\|_{L^2(a,b)}$$

since this is what we need to show (2.4). These new constraints are still convex, and the same proof works and yields a minimizer (u_0, v_0) with

$$\|\phi_{v_0}\|_{L^2(a,b)} \le \|T\|_{L^2(a,b)} \quad \text{and} \quad \|\phi_{f-k*(u_0+v_0)}\|_{L^2(a,b)} \le \|N\|_{L^2(a,b)}.$$

Unconstrained version. We will now realize the constraints by using the log barrier function (e.g., [39]). This will give us an unconstrained minimization problem corresponding to the proposed constrained minimization problem. We define $\mathcal{F}_{un}$ by

$$\begin{aligned}\mathcal{F}_{un}(u,v) = \|u\|_{\mathcal{BV}} + \lambda \int_{\mathbb{R}^n} |f - k * (u+v)|^2 \\ - \frac{\mu}{b-a}\int_a^b \ln(T^2(s) - \phi_v^2(s))ds \\ - \frac{\gamma}{b-a}\int_a^b \ln(N^2(s) - \phi^2_{f-k*(u+v)}(s))ds\end{aligned}$$

and solve

$$\inf_{u,v} \mathcal{F}_{un}(u,v). \tag{2.14}$$

It is easy to see that the functional $\mathcal{F}_{un}$ is convex in u and v by checking that the log barrier terms are convex. For $\lambda \in (0,1)$ and feasible points (u_1, v_1) and (u_2, v_2), we obtain that

$$\begin{aligned}T^2(s) - \phi^2_{\lambda v_1 + (1-\lambda)v_2}(s) &\geq \lambda(T^2(s) - \phi^2_{v_1}(s)) + (1-\lambda)(T^2(s) - \phi^2_{v_2}(s)) \geq 0 \\ \Leftrightarrow -\ln(T^2(s) - \phi^2_{\lambda v_1 + (1-\lambda)v_2}(s)) &\leq -\ln(\lambda(T^2(s) - \phi^2_{v_1}(s)) + (1-\lambda)(T^2(s) - \phi^2_{v_2}(s))) \\ &\leq -\lambda \ln(T^2(s) - \phi^2_{v_1}(s)) - (1-\lambda)\ln(T^2(s) - \phi^2_{v_2}(s)).\end{aligned}$$

In the same way, we obtain that

$$\begin{aligned}&-\ln(N^2(s) - \phi^2_{\lambda(f-k*(u_1+v_1))+(1-\lambda)(f-k*(u_2+v_2))}(s)) \\ &\leq -\lambda \ln(N^2(s) - \phi^2_{f-k*(u_1+v_1)}(s)) - (1-\lambda)\ln(N^2(s) - \phi^2_{f-k*(u_2+v_2)}(s)).\end{aligned}$$

Remark 7. In formulating an unconstrained problem, we can use $\ln(T^p(s) - \phi_v^p(s))$ instead of $\ln(T^2(s) - \phi_v^2(s))$ for any $1 \leq p < \infty$, which realizes the same constraint:

$$\phi_v^p(s) \leq T^p(s) \quad \text{a.e.} \;\Leftrightarrow\; \phi_v(s) \leq T(s) \quad \text{a.e.}$$

Likewise, we can make the same change to the last term. However, we choose $p = 2$ for numerical reasons.

Theorem 2.8. *Under the same assumptions as in Theorem 2.7, if there exists* $(u^*, v^*) \in \mathcal{BV}(\mathbb{R}^n) \times \cap_{a<s<b}\dot{H}^s(\mathbb{R}^n)$ *satisfying* $\mathcal{F}_{un}(u^*, v^*) < \infty$, *then* (2.14) *has a minimizer in* $\mathcal{BV}(\mathbb{R}^n) \times \cap_{a<s<b}\dot{H}^s(\mathbb{R}^n)$.

Proof. First, the assumption that $\mathcal{F}_{un}(u^*, v^*) < \infty$ for some (u^*, v^*) implies

$$\begin{aligned}-\infty < -\ln\left(\frac{1}{b-a}\int_a^b T^2(s)ds\right) \leq \frac{1}{b-a}\int_a^b -\ln(T^2(s))ds \\ \leq \frac{1}{b-a}\int_a^b -\ln(T^2(s) - \phi^2_{v^*}(s))ds < \infty\end{aligned}$$

and

$$-\infty < -\ln\left(\frac{1}{b-a}\int_a^b N^2(s)ds\right) \le \frac{1}{b-a}\int_a^b -\ln(N^2(s))ds$$
$$\le \frac{1}{b-a}\int_a^b -\ln(N^2(s)-\phi^2_{f-k*(u^*+v^*)}(s))ds < \infty.$$

Note that this means that $T^2 > 0$ and $N^2 > 0$ a.e. in (a,b). Hence, the functional $\mathcal{F}_{un}$ is bounded below, which enables us to extract a minimizing sequence. Now let $\{(u_k,v_k)\}_{k=1}^{\infty}$ be a minimizing sequence of (2.14). Then, we have $\phi^2_{v_k} \le T^2$ and $\phi^2_{f-k*(u_k+v_k)} \le N^2$ a.e. in (a,b), which guarantees (2.4) and (2.13), and the rest of the proof is the same as that of Theorem 2.7. ■

3. Numerical computations.

We present in this section a few numerical results for image restoration. Images are corrupted by either an averaging kernel or a Gaussian kernel, and then noise is added. Our main focus is on deblurring and Gaussian noise removal.

3.1. Numerical algorithm description.

We consider a grayscale image f as a scalar function from a domain $\Omega \subset \mathbb{R}^2$ to $\mathbb{R}$. When we solve the partial differential equations given below, impose periodic boundary conditions, and consider that 2Ω is the actual periodic domain.

One of the fundamental assumptions in our work is the existence of two universal functions T and N, as mentioned earlier. We obtain T by taking the average of the Sobolev norm profiles of texture from several randomly chosen texture images shown in Figure 1 for all the experiments in this paper. N is obtained from noise in the same way.

We solve (2.14) numerically using gradient descent and finite differences. We note that other more efficient methods could be used. Let us first write a semidiscrete version of the energy in (2.14), discretizing the s values:

$$\begin{aligned}\inf_{u,v}\mathcal{F}(u,v) = \|u\|_{\mathcal{BV}} &+ \lambda\int_{\mathbb{R}^n}|f-k*(u+v)|^2 \\ &- \frac{\mu}{K}\sum_{i=1}^{K}\ln\left(T^2(s_i) - \int_{\mathbb{R}^n} C^{2s_i}|\xi|^{2s_i}|\hat{v}|^2\right) \\ &- \frac{\gamma}{K}\sum_{i=1}^{K}\ln\left(N^2(s_i) - \int_{\mathbb{R}^n} C^{2s_i}|\xi|^{2s_i}|\hat{f}-\hat{k}(\hat{u}+\hat{v})|^2\right)\end{aligned} \tag{3.1}$$

for some $K > 0$ and $a = s_1 < s_2 < \cdots < s_{K-1} < s_K = b$. If we choose a large number $K > 0$, then the computational time for one iteration will be long due to the fact that the number of Fourier and inverse Fourier transforms that we need to compute is proportional to K. Hence, all our computational results use $-5 = a < b = -0.2 \le 0$, and we test several values of $K = 2, 5, 9, 17, 33$ to see the quality of the restored images as a function of K. Later, we show the results comparing different values of K in Table 3.

We now summarize the procedure for solving (3.1). Step 2 is stopped as soon as the energy functional stops decreasing or the computed noise variance becomes less than the true noise variance. In addition, we preset the maximum number of iterations for Step 2 to avoid

running the algorithm for a long time. A few hundred iterations works well. We adjust λ and Δt in Step 3 to keep the computed noise variance to at most the given noise variance when the algorithm stops (because a computed noise variance larger than expected may imply that some oscillatory features are not recovered in the texture component v).

Step 1. We start with $\Delta t = 0.3$. (λ, μ, γ) and the s values are as given. The initial guess (u_0, v_0) is $(G * f, 0)$, where G is a Gaussian function.

Step 2. We solve (3.1) by gradient descent for a certain amount of time as described above. While minimizing the functional, we check the variance of the computed noise. The computed noise variance is

$$\sigma_c^2 = \frac{1}{|\Omega|}\int_\Omega |f - k * (u+v)|^2,$$

and Step 2 is stopped before the preset maximum number of iterations if $\sigma_c^2 < \sigma^2$, where σ^2 is the given variance, or if the functional stops decreasing.

Step 3. If $\sigma_c^2 < \sigma^2$, then we use 0.8λ instead of λ and $0.6\Delta t$ instead of Δt.
If $\sigma_c^2 \geq \sigma^2$, then we only change Δt to $0.8\Delta t$.

Step 4. With the new set of parameters, we go to Step 2 and repeat this procedure five times.

Repeating five times at Step 4 was chosen for an empirical reason. Although three times was sufficient for good quality recovery, we wanted to ensure a sufficient improvement in the reconstruction while satisfying $\sigma_c^2 \sim \sigma^2$.

We give here the details of the gradient descent method used in Step 2. First, we obtain the formal Euler–Lagrange equations as follows:

$$\begin{aligned}
&\lim_{\epsilon\to 0}\frac{\mathcal{F}(u+\epsilon g, v+\epsilon h) - \mathcal{F}(u,v)}{\epsilon}\\
&= -\int \operatorname{div}\left(\frac{\nabla u}{|\nabla u|}\right) g - 2\int (\lambda k^* * (f - k*(u+v)) + \gamma \Re e\{R^\vee\})g\\
&\quad - 2\int (\lambda k^* * (f - k*(u+v)) + \Re e\{\gamma R^\vee - \mu Q^\vee\})h,
\end{aligned}$$

where g and h are test functions and k^* is the adjoint of k. Also, $Q^\vee$ and $R^\vee$ are the inverse Fourier transforms of Q and R, respectively. These are defined by

$$\begin{aligned}
Q(\xi) &= \left(\frac{1}{b-a}\int_a^b \frac{C^{2s}|\xi|^{2s}}{T^2(s) - \phi_v^2(s)} ds\right)\hat{v}(\xi),\\
R(\xi) &= \left(\frac{1}{b-a}\int_a^b \frac{C^{2s}|\xi|^{2s}}{N^2(s) - \phi^2_{f-k*(u+v)}(s)} ds\right)\bar{\hat{k}}(\xi)(\hat{f}(\xi) - \hat{k}(\xi)(\hat{u}(\xi) + \hat{v}(\xi))).
\end{aligned}$$

Then, the formal Euler–Lagrange equations are

$$\begin{aligned}
\operatorname{div}\left(\frac{\nabla u}{|\nabla u|}\right) + 2\lambda k^* * (f - k*(u+v)) + 2\gamma \Re e\{R^\vee\} = 0,\\
\lambda k^* * (f - k*(u+v)) + \Re e\{\gamma R^\vee - \mu Q^\vee\} = 0,
\end{aligned}$$

and we will eventually solve the following time-dependent system of PDEs by the finite difference scheme and the gradient descent method:

$$\begin{cases} \frac{\partial u}{\partial t} = \operatorname{div}\left(\frac{\nabla u}{|\nabla u|}\right) + 2\lambda k^* * (f - k * (u+v)) + 2\gamma \Re e\{R^\vee\}, \\ \frac{\partial v}{\partial t} = \lambda k^* * (f - k * (u+v)) + \Re e\{\gamma R^\vee - \mu Q^\vee\}. \end{cases} \tag{3.2}$$

When we compute the inverse Fourier transforms $R^\vee$ and $Q^\vee$, since 2Ω is the periodic domain, we first extend the functions R and Q to 2Ω by reflection, then compute $R^\vee$ and $Q^\vee$, and consider $R^\vee|_\Omega$ and $Q^\vee|_\Omega$. More details about the implementation involving inverse Fourier transforms on a periodic domain 2Ω are presented in prior work [27]. Let us briefly mention how we discretize each term in (3.2). The divergence term is approximated by

$$\operatorname{div}\left(\frac{\nabla u}{|\nabla u|}\right) \approx \frac{1}{4}\sum_{i,j=0}^{1}\left\{D_i^1\left(\frac{D^1_{(1-i)}u}{|D^1_{(1-i)}u|}\right) + D_j^2\left(\frac{D^2_{(1-j)}u}{|D^2_{(1-j)}u|}\right)\right\},$$

where D_0^l, D_1^l for $l = 1, 2$ are the forward and backward differences in the lth component, for instance,

$$D_0^1 u(i,j) = \frac{u(i+1,j) - u(i,j)}{h}.$$

To avoid division by zero, we add a small parameter $\epsilon > 0$ to the denominators in the above approximation of the divergence term. Since we assume a periodic boundary condition, we can use the MATLAB function IMFILTER to compute convolutions; e.g.,

$$k * (u+v) = IMFILTER(u+v, k, \text{'symmetric'}, \text{'conv'}).$$

Finally, the Sobolev norm $\|v\|_{\dot{H}^s}$ is computed as follows:

$$IFFT\left(ISHIFT\left(\left(C\pi\sqrt{\xi_1^2+\xi_2^2}\right)^s SHIFT(FFT(v))\right)\right).$$

Since we are taking negative values of s, when we evaluate the Sobolev norm, we set the value at the origin in the frequency domain to be 0.

To compare our method with prior methods, we compute the SNR (signal-to-noise-ratio) and the RMSE (root-mean-squared-error), which are defined by

$$\text{SNR}(\text{damaged image}(f), \text{original clean image}(g)) = 10\log_{10}\left(\frac{\text{Variance of } g}{\text{Variance of } f}\right),$$

$$\text{RMSE}(\text{damaged image}(f), \text{original clean image}(g)) = \sqrt{\frac{1}{|\Omega|}\sum_{(i,j)\in\Omega}(f(i,j) - g(i,j))^2}.$$

A bigger SNR value implies better recovery. The RMSE works in the opposite way; that is, a smaller RMSE value implies better recovery. Table 1 below compares the SNR and RMSE values for various experiments. The authors in [27] chose parameters that experimentally gave the best possible results. Hence, we also tried to find the most suitable parameters λ, μ, γ which produce the best results.

3.2. Performance of our method and comparison results. We will use two images, the factory image and the fishing boat image, for all the experiments because there are many previous restoration results (e.g., in [24], [27], [48]) that can be used for comparison. The initial time step Δt is 0.3, and the other parameters (λ, μ, γ) are $(1.32, 10^{-9}, 10^{-7})$ for the factory image and $(0.4, 10^{-9}, 10^{-7})$ for the fishing boat image.

Figures 3–5 are results obtained by the proposed method with different σ values. These are compared with previous results from [27] and [48]. Table 1 compares the results of the proposed model with those for the model in [27] in terms of SNR and RMSE values. The

Figure 3. *Top row (left to right): Noisy blurry image (f) with $\sigma = 1.1531$, restored image ($u + v$) using the proposed method, computed noise ($f - k * (u + v)$). Bottom row (left to right): Cartoon part (u), texture part (v). $SNR = 13.7362$, $RMSE = 8.6380$.*

Table 1
SNR and RMSE values for the results in Figures 3–6.

	SNR values			RMSE values		
	$\sigma = 1.1531$	$\sigma = 3$	$\sigma = 5$	$\sigma = 1.1531$	$\sigma = 3$	$\sigma = 5$
Noisy blurry (f)	8.9919	8.8371	8.5476	14.9153	15.3067	15.8254
Recovered ($u + \Delta g$) using TV/Sobolev [27]	13.5818	11.8415	10.6843	8.8643	10.8308	12.3742
Recovered ($u + v$) using proposed model	13.7362	12.2085	11.3058	8.6380	10.3827	11.5198

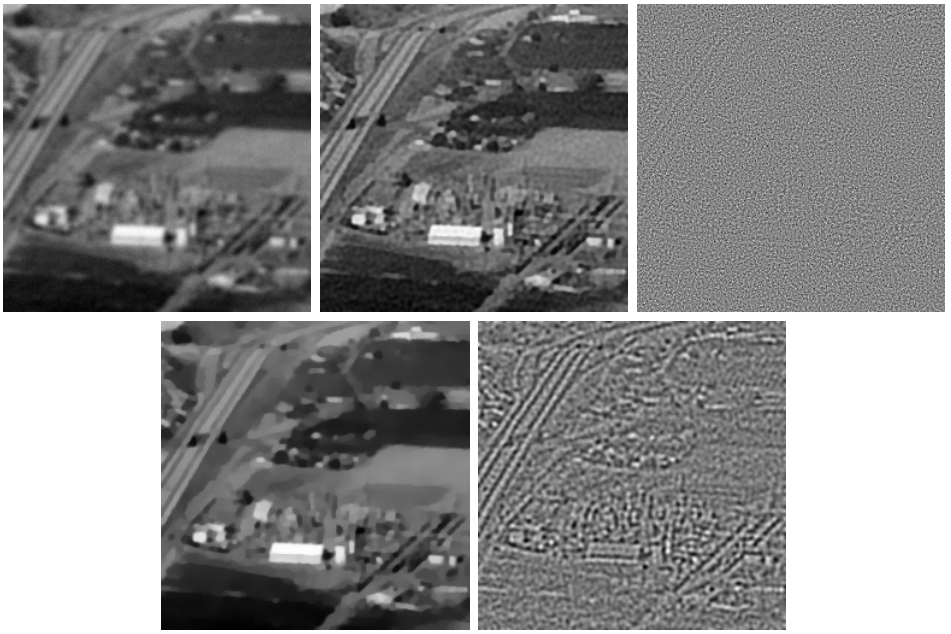

Figure 4. *Top row (left to right): Noisy blurry image (f) with $\sigma = 3$, restored image ($u + v$) using the proposed method, computed noise ($f - k*(u+v)$). Bottom row (left to right): Cartoon part (u), texture part (v). $SNR = 12.1351$, $RMSE = 10.3865$.*

Figure 5. *Top row (left to right): Noisy blurry image (f) with $\sigma = 5$, restored image ($u + v$) using the proposed method, computed noise ($f - k*(u+v)$). Bottom row (left to right): Cartoon part (u), texture part (v). $SNR = 11.3555$, $RMSE = 11.3619$.*

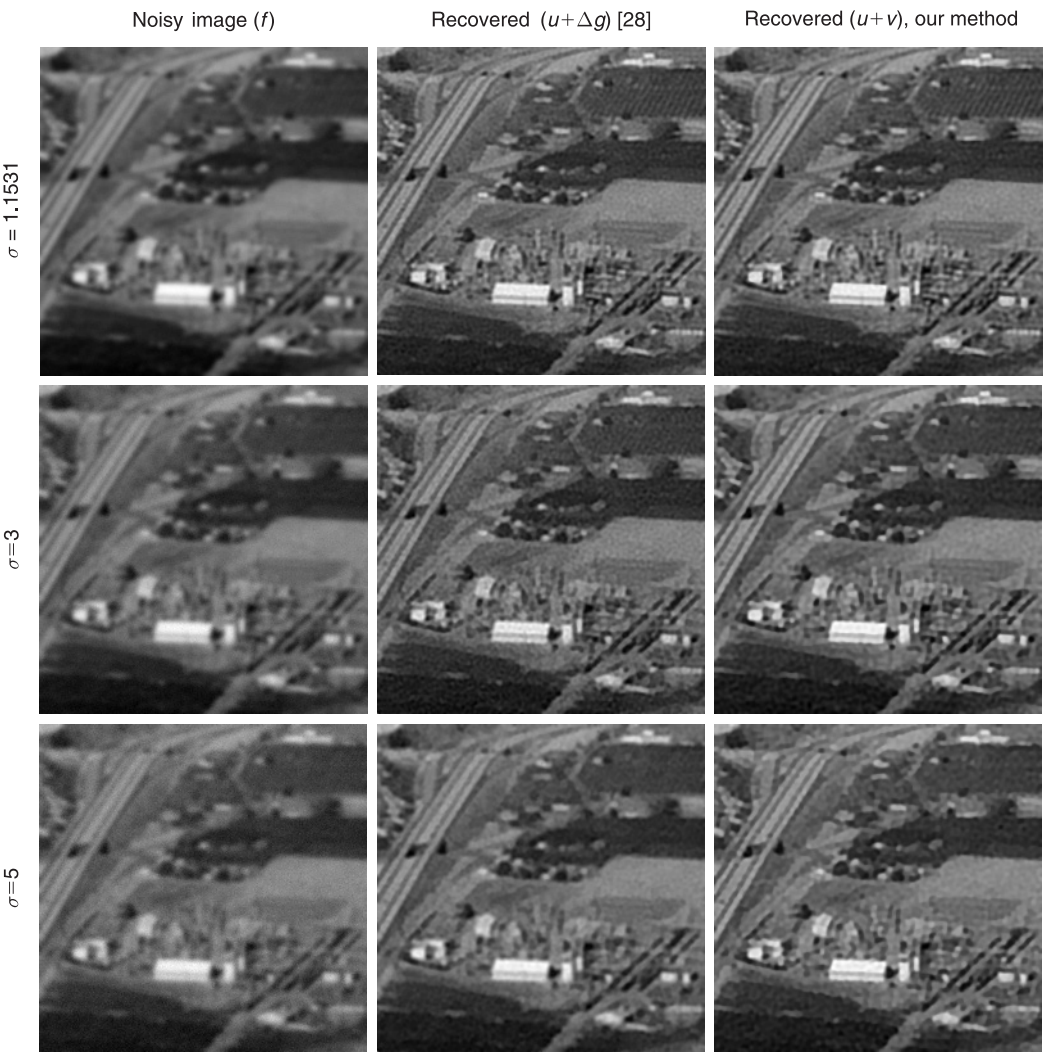

Figure 6. *Top row: With noise variance* $\sigma = 1.1531$*, the TV/Sobolev model from* [27] *gives* $SNR = 13.5818$*,* $RMSE = 8.8643$ *(*$\sigma = 1.1531$*,* $s = 0$*,* $p = 1$*), while our proposed model gives* $SNR = 13.7362$*,* $RMSE = 8.6380$ *(*$\sigma = 1.1531$*). Middle row: With noise variance* $\sigma = 3$ *the TV/Sobolev model from* [27] *gives* $SNR = 11.8415$*,* $RMSE = 10.8308$ *(*$\sigma = 3$*,* $s = 0$*,* $p = 3$*), while our proposed model gives* $SNR = 12.1351$*,* $RMSE = 10.3865$ *(*$\sigma = 3$*). Bottom row: With noise variance* $\sigma = 5$*, the TV/Sobolev model from* [27] *gives* $SNR = 10.6843$*,* $RMSE = 12.3742$ *(*$\sigma = 5$*,* $s = 0$*,* $p = 3$*), while our proposed model gives* $SNR = 11.3555$*,* $RMSE = 11.3619$ *(*$\sigma = 5$*).*

related images for the comparison are shown in Figure 6. We can see in Figure 6 that, by the proposed method, texture is better recovered and edges are sharper.

Besides the better recovery observed by comparing SNR and RMSE values, the proposed model has one more advantage over the model in [27], which also uses Sobolev spaces of negative differentiability. The algorithm we use in this paper is much like the one in [27]; however, model (2.3) utilizes the known values $T(s)$ and $N(s)$ for texture and noise, which

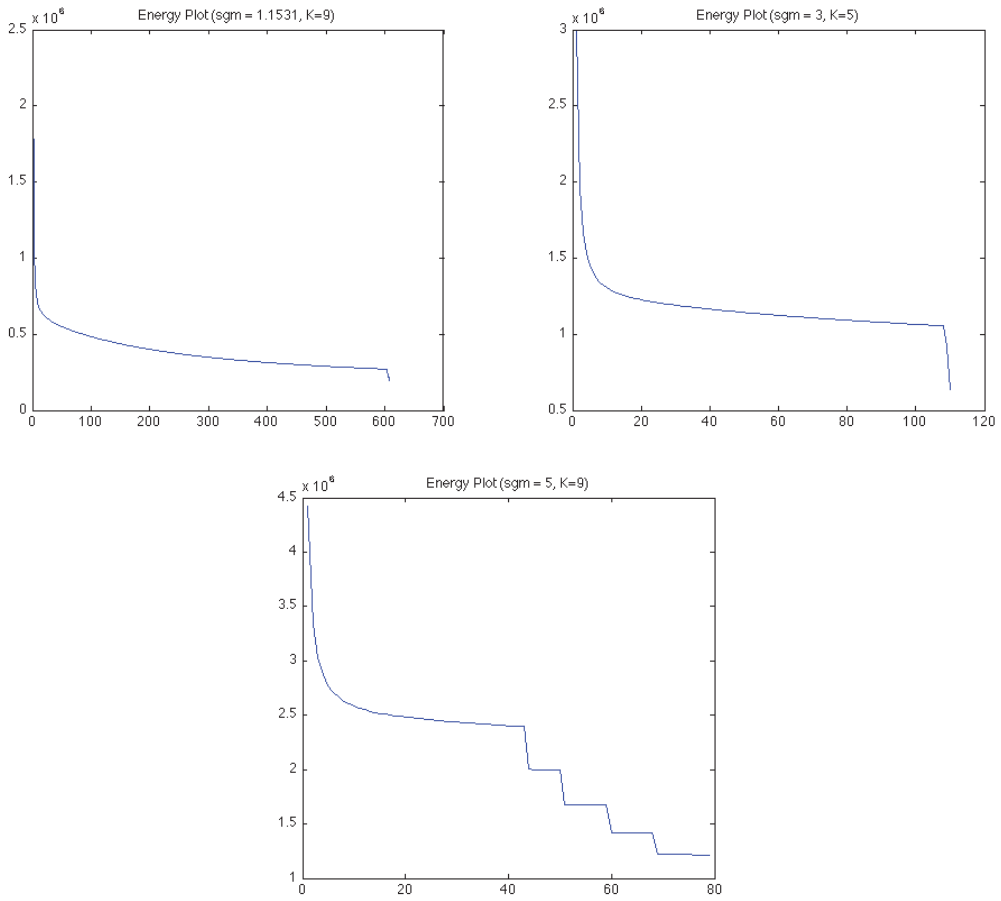

Figure 7. *Energy plots corresponding to the results in Figures 3–5.*

naturally imposes some restrictions on the computations of the texture and the noise components. The main focus of the algorithm in [27] was to match the known noise variance σ^2 and the computed noise variance σ_c^2 by adjusting the parameter λ accordingly. That is, Steps 3 and 4 above were very important in [27] since the choice of parameters much influenced the recovery. In particular, if we did not properly adjust λ in [27], then noise would get amplified easily and be absorbed into the texture component. On the other hand, the proposed model does not seem to rely on Steps 3 and 4 as much as the one in [27] does. Instead, $T(s)$ and $N(s)$ play the main role of controlling texture and noise, which makes the recovery somewhat insensitive to the adjustment of λ. In this sense, we do not observe the same difficulty in the computation of the proposed model as for the one in [27]. Figure 7 shows the energy over time for the proposed model and provides visual evidence for these observations: the steep drops at the tails indicate that Δt and λ have been changed according to Steps 3 and 4, resulting in decreasing the functional values. We should note that λ gets reduced only if the computed noise variance σ_c^2 is less than the noise variance σ^2, so updating λ results in decreasing the functional values as well. If we look at the plots horizontally, after the drops we hardly see

any changes in the functional values. In terms of SNR, we observe increases of the SNR values through these additional steps (Steps 3 and 4); however, the improvements are not so significant. As explained in the algorithm, we confirm in Table 2 that the proposed model removes noise of variance no bigger than the given variance σ^2.

Table 2

Comparison between the noise variances.

	Figure 3	Figure 4	Figure 5
Given noise variance	$\sigma = 1.1531$	$\sigma = 3$	$\sigma = 5$
Computed noise variance	$\sigma_c = 1.0633$	$\sigma_c = 2.8296$	$\sigma_c = 4.7398$

Table 3 shows the dependence of the quality of recovery on K. The SNR and RMSE values are very close in all cases. Intuitively speaking, the larger K is, the better the recovery should be. This was true among $K = 2, 5, 9$; however, it was not true among $K = 9, 17, 33$. The quality of recovery with $K = 17, 33$ may be related either to the increasing computational complexity of the algorithm causing trouble in obtaining optimal solutions or to the estimates of T and N.

Table 3

K is the number of s values being used in computations, which were uniformly chosen from $[-5, -0.2]$ including the endpoints.

	$K = 2$	$K = 5$	$K = 9$	$K = 17$	$K = 33$
SNR	11.3323	11.3227	11.3555	11.3064	11.2835
RMSE	11.3923	11.4049	11.3619	11.4262	11.4564

Figure 8, Figure 9, and Table 4 show the last comparison results that we performed. The authors of [24] reported the performances of various well-known effective regularizers for image show restoration. It turns out from this comparison that modeling the oscillatory component as in the present paper improves the recovery.

Figure 8. *Left to right: Noisy blurry image (f) with the same blurring kernel and the same noise ($\sigma = 5$) as in [24], restored image ($u + v$) from our proposed model, computed noise ($f - k * (u + v)$). $SNR = 14.1237$, $RMSE = 8.8481$.*

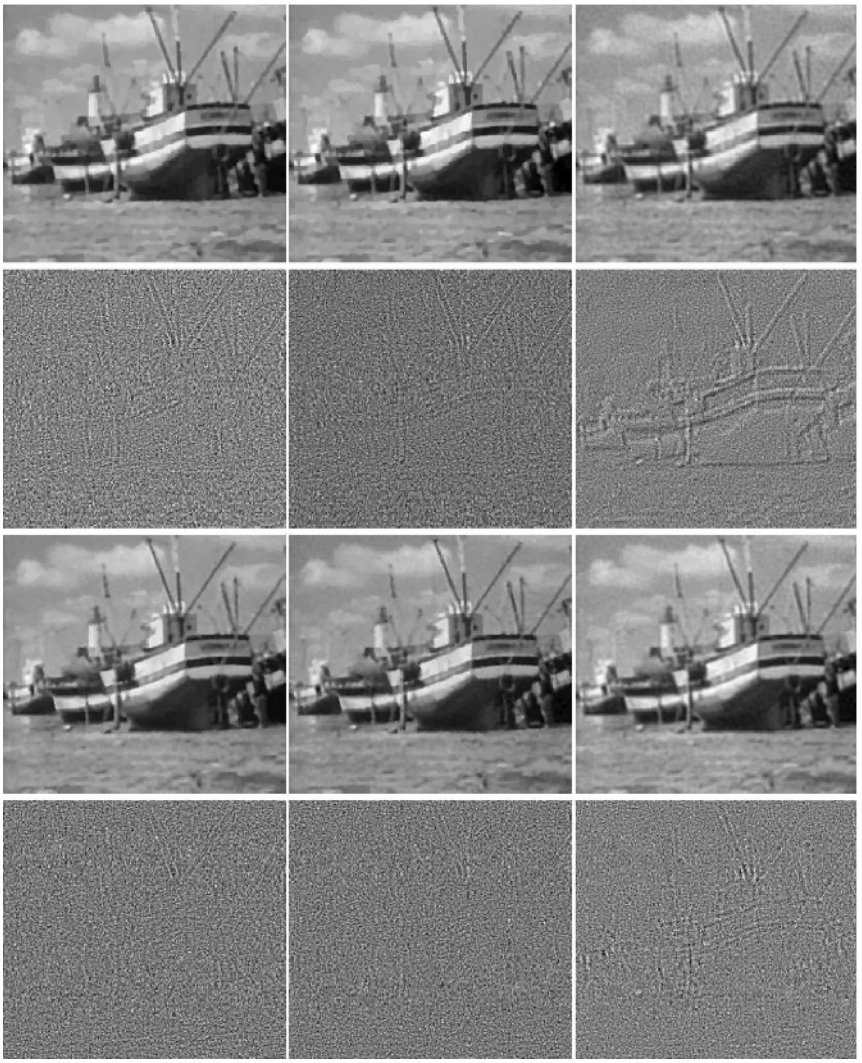

Figure 9. *Comparison with results in* [24]: *Recovery of noisy blurry image. First row: Recovered image (u) using TV ($SNR = 12.5115$), MSTV ($SNR = 12.5984$), MSH1 ($SNR = 11.5662$). Third row: Recovered image (u) using NL/TV ($SNR = 13.2277$), NL/MSTV ($SNR = 13.2348$), NL/MSH1 ($SNR = 12.3582$). The second and the fourth rows are computed noise for the corresponding reconstructions. See more details in* [24].

Table 4

SNR values for the results in Figures 8–9. TV: Total variation regularizer, MS: Mumford–Shah regularizer, H1: H1 norm regularizer, NL: Nonlocal means regularizer. See more details about the other results in [24].

	Our model	TV	MSTV	MSH1	NL/TV	NL/MSTV	NL/MSH1
SNR	14.1237	12.5115	12.5984	11.5662	13.2277	13.2348	12.3582

4. Conclusion. We have proposed a "cartoon+texture" minimization model to recover images degraded by blur and noise by separating noise from texture with the help of Sobolev norms. Unlike the previous attempts at such recovery in the literature, we have devised a

mathematical object which may be used to describe the difference between texture and noise. The cartoon component u is modeled as usual by a function of bounded variation, while the texture v and the noise $f - k * (u + v)$ are modeled by functions in a series of Sobolev spaces of negative differentiability $\dot{H}^s(\Omega)$ for $a < s < b < 0$. The recovered image is $u + v$. We numerically observed that the Sobolev norms of textured images, as functions belonging to $\dot{H}^s(\Omega)$ for $a < s < b < 0$, behave very similarly, which led us to our main assumption of the existence of functions T and N that describe such behaviors for texture and noise. Incorporated into the restoration model, T and N control the amount of texture and noise recovered, as opposed to the fixed or adjusted parameters controlling especially the noise. This partially solved the stability problem in the computational part as well. As our numerical results show, by a simple minimization we were able to ensure that the computed noise level was comparable to the given noise level while recovering as much texture as possible and keeping sharper edges. Comparisons with existing restoration results from [24], [27], [48] show that the proposed model provides improvement.

REFERENCES

[1] R. Acar and C. R. Vogel, *Analysis of bounded variation penalty methods for ill-posed problems*, Inverse Problems, 10 (1994), pp. 1217–1229.

[2] L. Alvarez, Y. Gousseau, and J. M. Morel, *Scales in natural images and a consequence on their bounded variation norm*, in Lecture Notes in Comput. Sci. 1682, Springer, New York, 1999, pp. 247–258.

[3] L. Alvarez, Y. Gousseau, and J. M. Morel, *The size of objects in natural and artificial images*, Adv. Imaging Electron Phys., 111 (1999), pp. 167–242.

[4] F. Andreu-Vaillo, V. Caselles, and J. M. Mazón, *Parabolic Quasilinear Equations Minimizing Linear Growth Functionals*, Progr. Math. 223, Birkhäuser-Verlag, Basel, Switzerland, 2004.

[5] P. Athavale and E. Tadmor, *Multiscale image representation using novel integro-differential equations*, Inverse Probl. Imaging, 3 (2009), pp. 693–710.

[6] G. Aubert and J. F. Aujol, *Modeling very oscillating signals. Application to image processing*, Appl. Math. Optim., 51 (2005), pp. 163–182.

[7] G. Aubert and L. Vese, *A variational method in image recovery*, SIAM J. Numer. Anal., 34 (1997), pp. 1948–1979.

[8] J. F. Aujol, G. Aubert, L. Blanc-Féraud, and A. Chambolle, *Image decomposition into a bounded variation component and an oscillating component*, J. Math. Imaging Vision, 22 (2005), pp. 1–88.

[9] J. F. Aujol and A. Chambolle, *Dual norms and image decomposition models*, Int. J. Computer Vision, 63 (2005), pp. 85–104.

[10] L. Bar, N. Kiryati, and N. Sochen, *Image deblurring in the presence of impulsive noise*, Int. J. Computer Vision, 70 (2006), pp. 279–298.

[11] L. Bar, N. Sochen, and N. Kiryati, *Semi-blind image restoration via Mumford-Shah regularization*, IEEE Trans. Image Process., 15 (2006), pp. 483–493.

[12] A. Buades, B. Coll, and J. M. Morel, *A review of image denoising algorithms, With a new one*, Multiscale Model. Simul., 4 (2005), pp. 490–530.

[13] A. Chambolle and P. L. Lions, *Image recovery via total variation minimization and related problems*, Numer. Math., 76 (1997), pp. 167–188.

[14] I. Daubechies and G. Teschke, *Variational image restoration by means of wavelets: Simultaneous decomposition, deblurring, and denoising*, Appl. Comput. Harmon. Anal., 19 (2005), pp. 1–16.

[15] I. Daubechies, G. Teschke, and L. Vese, *Iteratively solving linear inverse problems under general convex constraints*, Inverse Probl. Imaging, 1 (2007), pp. 29–46.

[16] S. Durand, F. Malgouyres, and B. Rougé, *Image de-blurring, spectrum interpolation and application to satellite imaging*, Control Optim. Calc. Var., 5 (2000), pp. 445–477.

[17] H. Fu, M. K. Ng, M. Nikolova, and J. L. Barlow, *Efficient minimization methods of mixed $\ell 2$-$\ell 1$ and $\ell 1$-$\ell 1$ norms for image restoration*, SIAM J. Sci. Comput., 27 (2006), pp. 1881–1902.
[18] J. B. Garnett, P. W. Jones, T. M. Le, and L. A. Vese , *Modeling oscillatory components with the homogeneous spaces $B\dot{M}O^{-\alpha}$ and $\dot{W}^{-\alpha,p}$*, Pure Appl. Math. Quart., 7 (2011), pp. 275–318.
[19] J. B. Garnett, T. M. Le, Y. Meyer, and L. A. Vese, *Image decompositions using bounded variation and generalized homogeneous Besov spaces*, Appl. Comput. Harmon. Anal., 23 (2007), pp. 25–56.
[20] S. Geman and D. Geman, *Stochastic relaxation, Gibbs distributions, and the Bayesian restoration of images*, IEEE Trans. Pattern Anal. Machine Intell., 6 (1984), pp. 721–741.
[21] G. Gilboa and S. Osher, *Nonlocal operators with applications to image processing*, Multiscale Model. Simul., 7 (2008), pp. 1005–1028.
[22] R. C. Gonzalez and R. E. Woods, *Digital Image Processing*, 3rd ed., Prentice–Hall, Englewood Cliffs, NJ, 2008.
[23] Y. Gousseau and J.-M. Morel, *Are natural images of bounded variation?*, SIAM J. Math. Anal., 33 (2001), pp. 634–648.
[24] M. Jung and L. Vese, *Nonlocal variational image deblurring models in the presence of Gaussian or impulse noise*, in SSVM '09: Proceedings of the Second International Conference on Scale Space and Variational Methods in Computer Vision, 2009, pp. 401–412.
[25] Y. Kim, J. Garnett, and L. Vese, *A convex minimization model in image restoration via one-dimensional Sobolev norm profiles*, in Proceedings of the 18th IEEE International Conference on Image Processing, 2011, pp. 701–704
[26] Y. Kim and L. A. Vese, *Functional minimization problems in image processing*, in Proc. SPIE 6814, C. A. Bouman, E. L. Miller, and I. Pollak, eds., SPIE, Bellingham, WA, 2008, pp. 68140Q-1–68140Q-11.
[27] Y. Kim and L. Vese, *Image recovery using functions of bounded variation and Sobolev spaces of negative differentiability*, Inverse Probl. Imaging, 3 (2009), pp. 43–68.
[28] S. Kindermann, S. Osher, and P. W. Jones, *Deblurring and denoising of images by nonlocal functionals*, Multiscale Model. Simul., 4 (2005), pp. 1091–1115.
[29] T. M. Le and L. A. Vese, *Image decomposition using total variation and* $\mathrm{div}(BMO)$, Multiscale Model. Simul., 4 (2005), pp. 390–423.
[30] S. Levine, *An adaptive variational model for image decomposition*, Lecture Notes in Comput. Sci. 3757, Springer, New York, 2005, pp. 382–397.
[31] L. Lieu, *Contribution to Problems in Image Restoration, Decomposition, and Segmentation by Variational Methods and Partial Differential Equations*, Ph.D. thesis, Department of Mathematics, UCLA, Los Angeles, CA, 2006.
[32] L. Lieu and L. Vese, *Image restoration and decomposition via bounded total variation and negative Hilbert-Sobolev spaces*, Appl. Math. Optim., 58 (2008), pp. 167–193.
[33] S. Lintner and F. Malgouyres, *Solving a variational image restoration model which involves L^∞ constraints*, Inverse Problems, 20 (2004), pp. 815–831.
[34] Y. Lou, X. Zhang, S. Osher, and A. Bertozzi, *Image recovery via nonlocal operators*, J. Sci. Comput., 42 (2010), pp. 185–197.
[35] F. Malgouyres, *Minimizing the total variation under a general convex constraint for image restoration*, IEEE Trans. Image Process., 11 (2002), pp. 1450–1456.
[36] F. Malgouyres, *A framework for image deblurring using wavelet packet bases*, Appl. Comput. Harmon. Anal., 12 (2002), pp. 309–331.
[37] Y. Meyer, *Oscillating Patterns in Image Processing and Nonlinear Evolution Equations*, Univ. Lecture Ser. 22, AMS, Providence, RI, 2001.
[38] D. Mumford and B. Gidas, *Stochastic models for generic images*, Quart. Appl. Math., 59 (2001), pp. 85–111.
[39] J. Nocedal and S. J. Wright, *Numerical Optimization*, Springer Ser. Oper. Res., Springer, New York, 1999.
[40] S. Osher, M. Burger, D. Goldfarb, J. Xu, and W. Yin, *An iterative regularization method for total variation-based image restoration*, Multiscale Model. Simul., 4 (2005), pp. 460–489.
[41] S. Osher, A. Solé, and L. Vese, *Image decomposition and restoration using total variation minimization and the H^{-1} norm*, Multiscale Model. Simul., 1 (2003), pp. 349–370.

[42] G. Peyré, S. Bougleux, and L. D. Cohen, *Non-local regularization of inverse problems*, Lecture Notes in Comput. Sci. 5304, Springer, New York, 2008, pp. 57–68.
[43] L. Rudin and S. Osher, *Total variation based image restoration with free local constraints*, in Proceedings of the IEEE International Conference in Image Processing, 1994, pp. 31–35.
[44] L. Rudin, S. Osher, and E. Fatemi, *Nonlinear total variation based noise removal algorithms*, Phys. D, 60 (1992), pp. 259–268.
[45] J. L. Starck, M. Elad, and D. L. Donoho, *Image decomposition via the combination of sparse representations and a variational approach*, IEEE Trans. Image Process., 14 (2005), pp. 1570–1582.
[46] E. Tadmor, S. Nezzar, and L. Vese, *A multiscale image representation using hierarchical* (BV, L^2) *decompositions*, Multiscale Model. Simul., 2 (2004), pp. 554–579.
[47] E. Tadmor, S. Nezzar, and L. Vese, *Multiscale hierarchical decomposition of images with applications to deblurring, denoising and segmentation*, Commun. Math. Sci., 6 (2008), pp. 281–307.
[48] H. Takeda, S. Farsiu, and P. Milanfar, *Deblurring using regularized locally-adaptive kernel regression*, IEEE Trans. Image Process., 17 (2008), pp. 550–563.
[49] A. N. Tikhonov, *On the stability of inverse problems*, Dokl. Akad. Nauk SSSR, 39 (1943), pp. 195–198.
[50] A. N. Tikhonov, *Solution of incorrectly formulated problems and the regularization method*, Soviet Math. Dokl., 4 (1963), pp. 1035–1038; Russian original in Dokl. Akad. Nauk SSSR, 151 (1963), pp. 501–504.
[51] A. N. Tikhonov and V. A. Arsenin, *Solution of Ill-posed Problems*, Winston & Sons, Washington, DC, 1977.
[52] L. Vese, *A study in the BV space of a denoising-deblurring variational problem*, Appl. Math. Optim., 44 (2001), pp. 131–161.
[53] L. A. Vese and S. J. Osher, *Modeling textures with total variation minimization and oscillating patterns in image processing*, J. Sci. Comput., 19 (2003), pp. 553–572.